Influence of the 11 year solar cycle on annual streamflow maxima in Southern Canada

Andreas Prokoph [a], Jan Adamowski [b,*], Kaz Adamowski [c]

[a] D
[b]
ç, ç , , , 1 6 5

ç :
Received 17 June 2011
Received in revised form 19 February 2012
Accepted 28 March 2012
Available online 4 April 2012
This manuscript was handled by Andras Bardossy, Editor-in-Chief, with the assistance of Luis E. Samaniego, Associate Editor

ç:
Solar cycle
Streamflow
Canada
Wavelet analysis
Floods
El Nino

S U M M A R Y

The re-occurrence pattern of major extremes in hydrology, such as the timing and intensity of river floods, is related to a variety of natural and anthropogenic factors. In this studisTIn
the wavlets
aalysiis
demo
cycnes
relaivkely
sunkspot numbesy

1. Introduction

The influence of variability in the solar irradiance and galactic cosmic ray flux on the surface temperature and precipitation variability of the Earth has often been considered negligible because the sun's output varies by only ~

linear oceanic-atmospheric responses, such as solar-intensity influence pressure anomaly perturbations and changing wind regimes (e.g., Hameed and Lee, 2005). There is also concern that 11-year streamflow cyclicity may spuriously arise from random or non-linear processes as demonstrated by a study of the Nile flood record in Egypt (for example Hurst, 1951; Koutsoyiannis, 2006).

One of the objectives of this study is to provide a better understanding of the potential link between 11 year sunspot cyclicity and the re-occurrence of large instant floods in multi-year time intervals. Most streamflow records are too short to determine the statistical significance of the average amplitudes (or spectral power) and stationarity (i.e. constant wavelength) of the detected periodicities. In this study, continuous wavelet analysis (Morlet et al., 1982) is used to extract wavelengths, magnitudes and phases of potential ~11 year (9–13 years) solar cyclicity. In contrast to

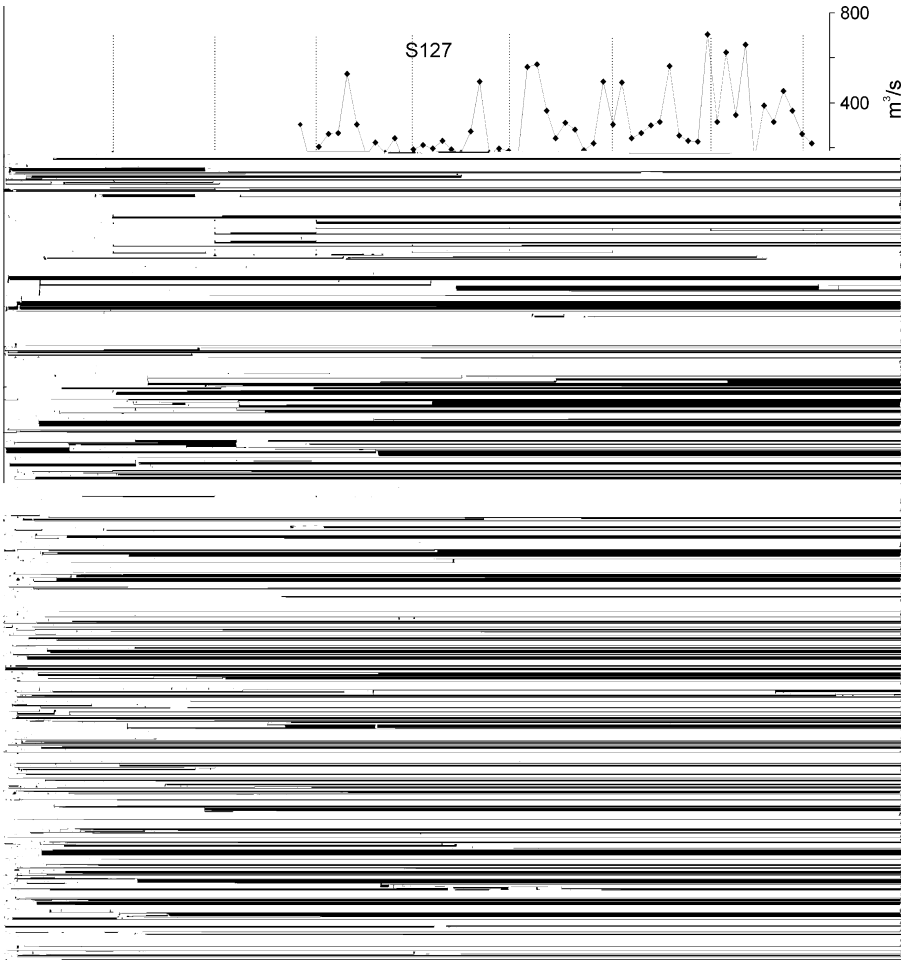

Fig. 2. Maximum annual streamflow (MAS) measurements (in m^3/s) in Southern Canada from 1923 to 1997 ordered from East (top) to West (bottom). Note: Available measurements are marked with a diamond symbol. Dotted vertical lines mark 10.5 year intervals.

selected wavebands, which is an issue of particular interest in this study. The wavelet coefficients of a time series (ϛ) with s referring to distance of, as in this study, time, are calculated by the convolution

$$_{\psi}(,) = \left(\frac{1}{\sqrt{}}\right)\int_{-\infty}^{\infty} (ϛ)\psi\left(\frac{ϛ - }{}\right) ϛ \quad (1)$$

where ψ is the mother wavelet; the variable is the scale factor that determines the characteristic frequency or wavelength; and represents the shift of the wavelet over (ϛ) (Chao and Naito, 1995). The wavelet coefficients are normalized to represent the amplitudes of Fourier frequencies by replacing $\sqrt{}$ with . The matrix of wavelet coefficients (,) form the so called 'scalogram', which is coded with shades of gray or colors for graphical expression.

In this study, the continuous wavelet transform with the Morlet wavelet as the mother function was used, which is simply a sinusoid with the wavelength/period modulated by a Gaussian function (Morlet et al., 1982). A parameter is used to modify the wavelet transform bandwidth resolution either in favor of time or in favor of frequency, because the bandwidth resolution for the wavelet transform varies with frequency resolution $\Delta = \frac{\sqrt{2}}{4\pi}$ with Δ referring to dilation in scale (or wavelength), and a location resolution $\Delta = \frac{}{\sqrt{2}}$ with Δ referring to dilation in time (or time-steps). For all analyzes = 6 was chosen, which gives sufficiently precise results in the resolution of depth and frequency, respectively (Ware and Thomson, 2000). The shifted and scaled Morlet mother wavelet that was used is defined as

$$\psi_{, ,}(ϛ) = \sqrt[4]{\pi}\sqrt{\quad} \; ^{-\frac{2\pi(ϛ-)}{}} \; ^{-\frac{1}{2}\left(\frac{ϛ-}{}\right)^2} \quad (2)$$

The wavelet analysis technique used in this article is explained in Prokoph and Barthelmes (1996).

The wavelet coefficients at the beginning and end of the data are subject to 'edge effects' because parts of the analysis windows are located outside of the data set. For the large analysis windows that are used for long wavelengths most of the analysis window can be located outside the range of the time series. Thus, the edge effects of the wavelet coefficients have a curved shape in the time frequency space, which is called the 'cone of influence' (Torrence and Compo, 1998). The edge effects have been compensated for by a normalization approach that is described in Adamowski et al. (2009).

Wavelet coefficients (i.e. amplitudes) and phases were extracted for the 8–13 year waveband of the streamflow records to evaluate the particular effect of this waveband on the overall streamflow data variability and its potential relation to ~11 year solar insulation variability. This is shown in the example for wavelet analysis of station S4 (Fig. 3B–D).

3.2. ϛ ~11 ϛ

The original time series can be completely reconstructed using the inverse wavelet transform (Grossman and Morlet, 1984; Holschneider et al., 1989)

$$(ϛ) = \int_0^{\max}\int_0^{\max} ( )\Psi\left[\frac{(ϛ -)}{}\right] \quad \frac{}{^2} \quad (3)$$

In this study only signals from the ~11 (8–13) year waveband were of interest for reconstruction. Thus, the reconstruction was reduced to narrow wavebands (8, 13 years) for a single component centred at = 11 years from the start of the time series set at = 0 to its end $_{max}$. The reconstructed data interval is set to = 1 year. Thus, the partial reconstruction in the (8, 13) year waveband results in the component time series (ʏ) as shown by

$$(ʏ) = \int_0^{max} ( )\Psi\left[\frac{(ʏ -)}{}\right] \quad (4)$$

The reconstructions of signal (ʏ) of component were further simplified by the inclusion of phase φ at each time ʏ for waveband centered at in the reconstruction equation

$$(ʏ) = ( )(\cos 2\pi ʏ/ + \phi\ (ʏ)) \quad (5)$$

with φ representing the phase at time ʏ. The partition of variability contributed by the 11-year cyclicity can be documented by reconstructing the ~11 year waveband and subtracting it from the complete records.

4. Results

Visual inspection indicates that the maximum annual streamflow (MAS) records appear to only occasionally follow a sharp 10.5 year re-occurrence pattern, such as can be seen in station S4 from 1964 to 1975 (Fig. 2). Moreover, the MAS variability is in gen-

discharges following the NAO/Southern Oscillation Index (SOI) change pattern along the coastlines (Currie and O'Brien, 1988; Pekárová et al., 2003; Labat et al., 2005). Wavelet analysis by Labat et al. (2005) also confirmed our observation that the NAO pattern influence varies temporally, being most strongly represented in the river discharge pattern around 1970. Cycles of 2–8 years are also commonly found in drought, precipitation and river discharge in North America and are commonly related to the El Nino/Southern Oscillation (ENSO) pattern (Oladipo, 1989; Gingras and Adamowski, 1995; Labat et al., 2005; Tardif et al., 1998). The weak

spot lows have also been detected in the Canadian Prairies (Garnett et al., 2006), which likely results in correspondingly higher flow levels in the two stations located on the Eastern Rocky Mountain/Prairies transition (foothills) where the significant sunspot influence had been detected.

The output of solar ultraviolet (UV) radiation varies by up to 4% during a typical 11-year solar cycle (in the 240–320 nm region) compared to the ~1% average solar energy fluctuations in the same cycle period (Lean, 2000; Gray et al., 2010). Thus, in particular, Montane regions that already receive more UV radiation in general than lowlands may receive significantly less solar energy as well as more precipitation due to more clouds during solar low years. This leads to more albedo, snow accumulation and a later but more abrupt onset of snowmelt and stronger floods in the year. The resulting precipitation cyclicity is likely enhanced by a positive feedback with (longer) snow accumulation and abrupt spring melt that leads to periodic 11 year floods in the Rocky Mountain region (Timoney et al., 1997). The maximum floods appear most often (~60%) during years with minimum sunspot numbers or one year before, about 4 years before the next and 7 years after the last sunspot maximum (Figs. 2, 3 and 6). The results of wavelet analysis also suggest that the maximum floods during an MAS cycle are stronger when the 11 year sunspot cycle is weaker. The number of records is too low to address significant risks for floods in the Montane Cordillera at minimum sunspot number years, but policy makers and water managers are advised to observe streamflows in this eco-zone more carefully during these episodes. Similarly, the observed high MAS during sunspot minima in Central Canada from a single, incomplete streamflow record (Figs. 2 and 6) cannot be considered significant enough to address the risk statistically. It is recommended that policy makers and other researchers carry out additional data analysis on the potential solar-flood link in this region as the Boreal Shield and the Great Plain cover large parts of North America. However, there is no long-term trend that is evident in the Montane eco-zone that could be related to long-term climate change.

6. Conclusions

The MAS in watersheds in Southern Canada can be related to 11 year solar cyclicity in regionally varying degrees. An approximately 11 year cyclicity is evident in all eco-zones but it is superimposed by much stronger NAO and ENSO related precipitation variability. The 11 year MAS cyclicity is strong in the Montane eco-zone (Rocky Mountains) and less significant in the Boreal Shield. In these eco-zones, high MAS (main floods) will most likely occur during low sunspot number years. The MAS are generally higher during weaker sunspot cycles.

Acknowledgment

Financial support for this study was provided by the Cyprus Institute as well as an NSERC grant held by Jan Adamowski.

References

Adamowski, J., 2008a. Development of a short-term river flood forecasting method for snowmelt driven floods based on wavelet and cross-wavelet analysis. Journal of Hydrology 353, 247–266.

Adamowski, J., 2008b. River streamflow forecasting using wavelet and cross-wavelet transform models. Journal of Hydrological Processes 22, 4877–4891.

Adamowski, K., Prokoph, A., Adamowski, J., 2009. Development of a new method of wavelet aided trend detection and estimation. Hydrological Processes 23, 2686–2696.

Alexander, W.J.R., Bailey, F., Bredenkamp, D.B., van der Merwe, A., Willemse, N., 2007. Linkages between solar activity, climate predictability and water resource development. Journal of the South African Institution of Civil Engineering 49, 32–44.

Carslaw, K.S., Harrison, R.G., Kirkby, J., 2002. Cosmic rays, clouds, and climate.

Svensmark, H., Friis-Christensen, E., 1997. Variation of cosmic ray flux and global cloud coverage - a missing link in solar-climate relationships. Journal of Atmospheric and Solar-Terrestrial Physics 59, 1225–1232.
Tardif, J., Dutilleul, P., Bergeron, Y., 1998. Variations in periodicities of the ring width